Characteristics of brightness temperature with respect to rain rate over ocean and land and its implication on rain rate retrieval

Diganta Kumar Sarma, Mahen Konwar & Sanjay Sharma
Department of Physics, Kohima Science College, Kohima, Nagaland 797 002, India
e-mail: sanjay_sharma11@hotmail.com
and
Jyotirmoy Das & Srimanta Pal
Electronics & Communication Sciences Unit, Indian Statistical Institute, Kolkata 700 035, India

Received 9 May 2005; revised 30 January 2006; accepted 23 March 2006

This paper studies the characteristics of brightness temperature (BT) with respect to rain rate over ocean and land and its subsequent implication on rainfall retrieval utilizing artificial neural network (ANN). The BTs data are obtained from Tropical Rainfall Measuring Mission (TRMM) Microwave Imager (TMI). Variations of BT with rain rate are compared for all the nine channels over ocean and land, and over ocean 10.67 GHz is found to be most sensitive to rain rate. For 37.0 GHz channels, emission effect is not noticed over land, but it is prominent over ocean for lower value of rain rate. Over land, lower frequency channels (Nos 1-4) are least sensitive to rain rate. From a quantitative comparison of the 85.5 GHz channels over ocean and land, BT difference of ~10 K is observed. It is also observed that polarization difference between the BTs for this frequency channel is more over ocean. A difference of ~10 K and ~3 K are noticed over ocean and land, respectively. Neural networks are trained over ocean and land to give rain rate as output. The nine channel BTs from TMI are considered as input for training the networks. The collocated near-surface rainfall rate data from TRMM precipitation radar are considered as target. Correlation values of 0.92 and 0.82 are observed for validation set over ocean and land, respectively, with root mean square error (rmse) values of 2.26 mm/h and 3.54 mm/h. It is observed that rain rate retrieval is better over land after discarding the lower frequency channels. The ANN retrieved rain rate is compared with TMI rain rate and correlations of 0.71 and 0.57 are observed over ocean and land, respectively.

Keywords: Brightness temperature, Rain rate, Rain rate retrieval, Precipitation radar, Artificial neural network.
PACS No.: 92.60 Jq; 92.60. Ry; 92.60 Nv
IPC Code: G01S 13/95; G06 T 1/40

1 Introduction

Brightness temperature[1] (BT) is the intensity of radiation emitted by earth surface and is obtained from remotely sensed radiometers. It is one of the most important parameters to study the global precipitation. The BT data are equally important in retrieving other important geophysical parameters such as sea surface temperature (SST), sea surface wind speed (SSW), water vapour content (WVC), cloud liquid water content (LWC), etc.

Remote sensing techniques can provide rainfall measurements, but accuracy is less compared to ground observations from rain gauge, disdrometer and radar. It has the advantage of providing rain retrieval over large area and particularly over ocean, which is not possible with ground-based instruments. Rainfall can be inferred from the radiation in visual, infrared and microwave (MW) regimes. The Tropical Rainfall Measuring Mission (TRMM) payload has represented a quantum leap with its five instruments, viz. TRMM microwave imager (TMI), precipitation radar (PR), visual and infrared sensor (VIRS), clouds and earth radiant energy system (CERES) and lightning imaging sensor (LIS) to explore the tropical rainfall characteristics. The passive and active sensors, TMI and PR respectively, provide an excellent opportunity to study the global precipitation due to their common swath of observations. The TMI senses the upwelling radiations at nine channels in five frequencies, i.e. 10.67, 19.35, 37.0 and 85.5 GHz with both horizontal and vertical polarization and 21.3 GHz with only vertical polarization. The PR, on the other hand, works at 13.8 GHz with dual frequency agility. The details of their scanning geometry can be found elswhere[2]. The VIRS gives rainfall characteristics through the cloud top information, as clouds are opaque at this fre-

quency range. The TMI, on the other hand, sensing BTs at MW frequencies are physically more directly related to rainfall due to its penetration through cloud.

Variations of BTs with surface rainfall at different frequencies are somewhat different over ocean and land due to their different emissivities (~0.4 and ~0.8 respectively). Sea surface has less emissivity, while raindrops are much more effective emitter and thus provides a good contrast against the sea surface as compared to land. Emission of radiations from atmospheric particles results in an increase of the signal received by the satellite sensor, while at the same time, the scattering due to hydrometeors reduces the radiation stream. At the lower part of rainfall rate, BTs increase due to the effect of absorption/emission. As rain rate increases, a saturation regime is reached where scattering balances emission, and at yet high rain rate, BTs decrease due to the weak scattering by the liquid hydrometeors[3]. But, for 10.67 GHz channels, saturation regime is not reached[4] thus showing strong linearity with BTs as compared to the other lower frequency channels. On the other hand, over land due to its high emissivity (~0.8), the lower frequency channels are less sensitive to the raindrops. But the higher frequency channels, sensing BTs due to scattering, are more useful for rainfall retrieval over land. This shows that, for rainfall retrieval, different models have to be considered over ocean and land. Petty[5] discussed the status of satellite based rainfall estimation over land.

The simplest microwave methods for rainfall retrieval are based on statistical regression using some of the BTs at different frequencies or the combination of them to derive a rain index, which is then related to rain rate. One example of such rain index is scattering index[6] (SI). There is another index known as normalized polarization difference[7] (NPD), which is based on theoretical considerations. In general, algorithms are differentiated according to their use over ocean and land. A combination of visible (VIS) and infrared (IR) data along with MW is useful for rainfall retrieval both over land and ocean[8-14]. An artificial neural network (ANN) technique also provides an efficient way for rain retrieval with MW as well as by combining IR and MW data[15-19].

The main objective of this paper is to study the characteristics of BTs as obtained from TMI with respect to rain rate both over ocean and land and its subsequent implications in rain rate retrieval utilizing ANN technique. Further, the retrieval accuracy is compared over ocean and land with the help of standard 2A12 rain rate. The nine channel BTs from TMI, ranging from 10.67 GHz to 85.5 GHz, are the input features. The collocated PR rainfall rate is considered as the desired or target values.

2 Data description and preparation

The data products utilized in this study are 2A25 (PR rain rate/PR-corrected reflectivity), 1B11 (TMI brightness temperature) and 2A12 (TMI surface rain rate). For PR data, the near-surface rainfall rate, which is defined as the rainfall rate at the lowest height free from ground clutter has been considered. Data set is prepared from the collocated measurements of the two sensors TMI and PR. In order to find the collocated pixels, latitude and longitude difference of ±0.04° between PR and all the nine channels of TMI have been chosen. As the effective field of view[2] (EFOV) along cross track (CT) is 9.1 km for the lower frequency channels, two PR pixels are averaged over that distance. Again for the 85.5 GHz channel EFOV CT is 4.6 km. Therefore, two consecutive pixels of TMI (85.5 GHz) and PR are averaged. For the down track direction, four PR pixels are averaged for the lower frequency channels. Data sets over ocean are considered for Pacific (21 Mar. 2000, Orbit No. 13322), Atlantic (20 July 2000, Orbit No. 15234) and Indian Ocean (28 May 2000, Orbit No. 14385) and over land, data sets for India (21 June 2000, Orbit No. 14775; 12 June 2000, Orbit No. 14632) and Eastern China (14 July, 2000 Orbit No. 15126; 17 May 2000, Orbit No. 14219) are considered.

3 Characteristics of brightness temperature (BT) over ocean and land

Characteristics of BT with respect to PR near-surface rainfall rate both over ocean and land are studied in this paper. Figure 1[(a)-(i)] shows the variation of BT with respect to PR near-surface rain rate over ocean. It can be noticed that, for the lower frequency channel [10.67 GHz (V and H)], BT is linearly increasing with rain rate showing the emission characteristic at this frequency. But for higher frequency channels (19.35 GHz), BT tends to saturate beyond rain rate of about 7 mm/h. For 21 GHz channel, which is responsible for water vapour, BT has less variation with rain rate. For 37.0 GHz channel, emission as well as scattering effect can be noticed. For lower rain rate, emission effect is responsible for increase in BT values, but as rain rate increases scat-

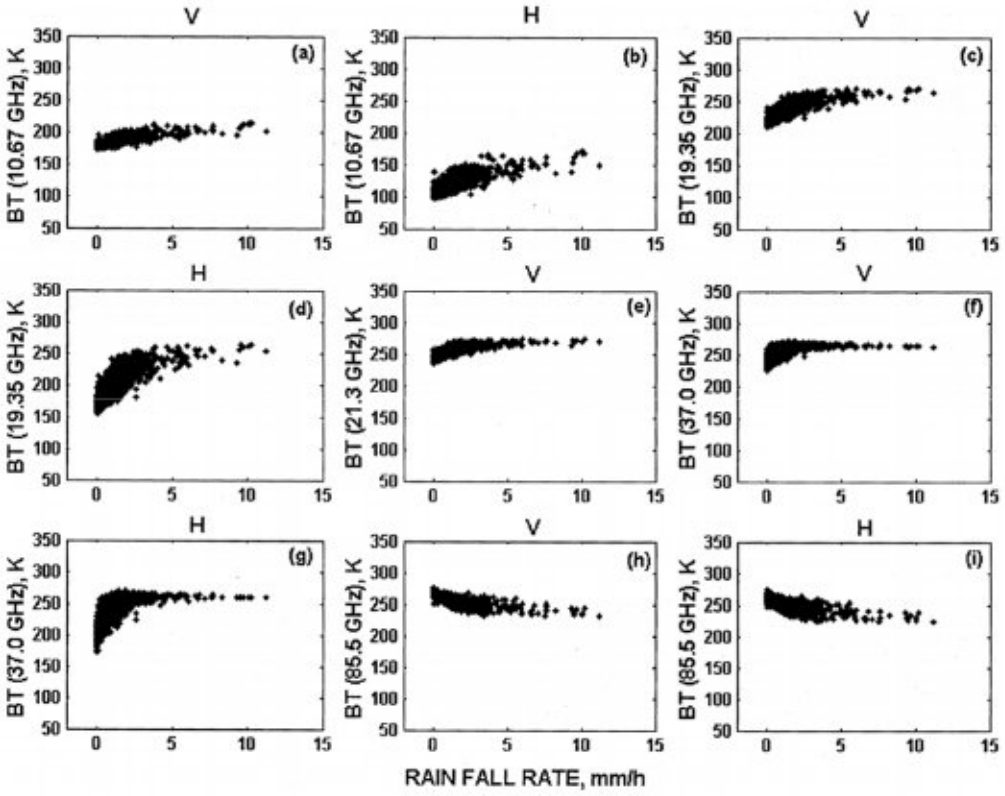

Fig. 1—Variations of BTs of nine channels with PR near-surface rain rate over ocean

tering effects dominate and it tends to reduce with rain rate. In between emission and scattering, there is a region called saturation regime where emission balances scattering[4]. On the other hand, for the 85.5 GHz channels, BT values are reduced where scattering effect dominates the radiation stream. At this frequency cloud is opaque, so the maximum scattering effect occurs due to ice scattering. Figure 2 [(a)-(i)] shows that, for lower frequency channels (10.67 GHz, 19.67 GHz both vertical and horizontal and 21.3 GHz), BTs have very less variation with rain rate. Only 37.0 and 85.5 GHz channels respond to rain rate. One point to be noted here is that, over land the emission effect for the 37.0 GHz channel is not noticed, whereas over ocean it is prominent for low rain rates. Though the use of lower frequency channels is limited for rainfall retrieval over land, the ice scattering signature from 85.5 GHz channel can be used as precipitation information though it is not direct (as 85.5 GHz channels mainly responds to ice present aloft). Figure 3 shows the pixel-wise spatial variations of BTs for all the frequencies with PR rain rate over land. It can clearly be noticed that lower frequency channels are not affected by rain, whereas BTs for 85.5 GHz horizontal channel ($BT_{85.5H}$) responded quite nicely to surface rain rate. The $BT_{85.5H}$ depression is clearly noticed for the high rain rate (for corresponding PR pixels 26-33) and for low rain $BT_{85.5H}$ has high value. Another important observation can be made from Fig. 3 is that, for 37.0 GHz channel, BT responds mainly to strong surface rain rate and is less sensitive towards the lower rain rate. That means, over land, only the scattering effect dominates for this frequency. Over land, the use of lower frequency channels are obscured due to the high emissivity of the surface. As land surface has very high emissivity (~0.8), it does not give good contrast to the rain above the surface as compared to that over ocean where sea surface is cool with less emissivity (~0.4). But for higher frequency channels (37.0 and 85.5 GHz) that are affected due to scattering mechanism can be used as rainfall estimator. Kidd[20] has also pointed out that whilst scattering can occur at 37.0 GHz, it has been difficult to extract low rainfall rates from data at this frequency, whereas 85.5 GHz is more sensitive to the scattering from smaller particles.

A quantitative comparison between BTs over ocean and land is also presented here. For that a linear fitting is performed on the BT data for 10.67 and 85.5 GHz

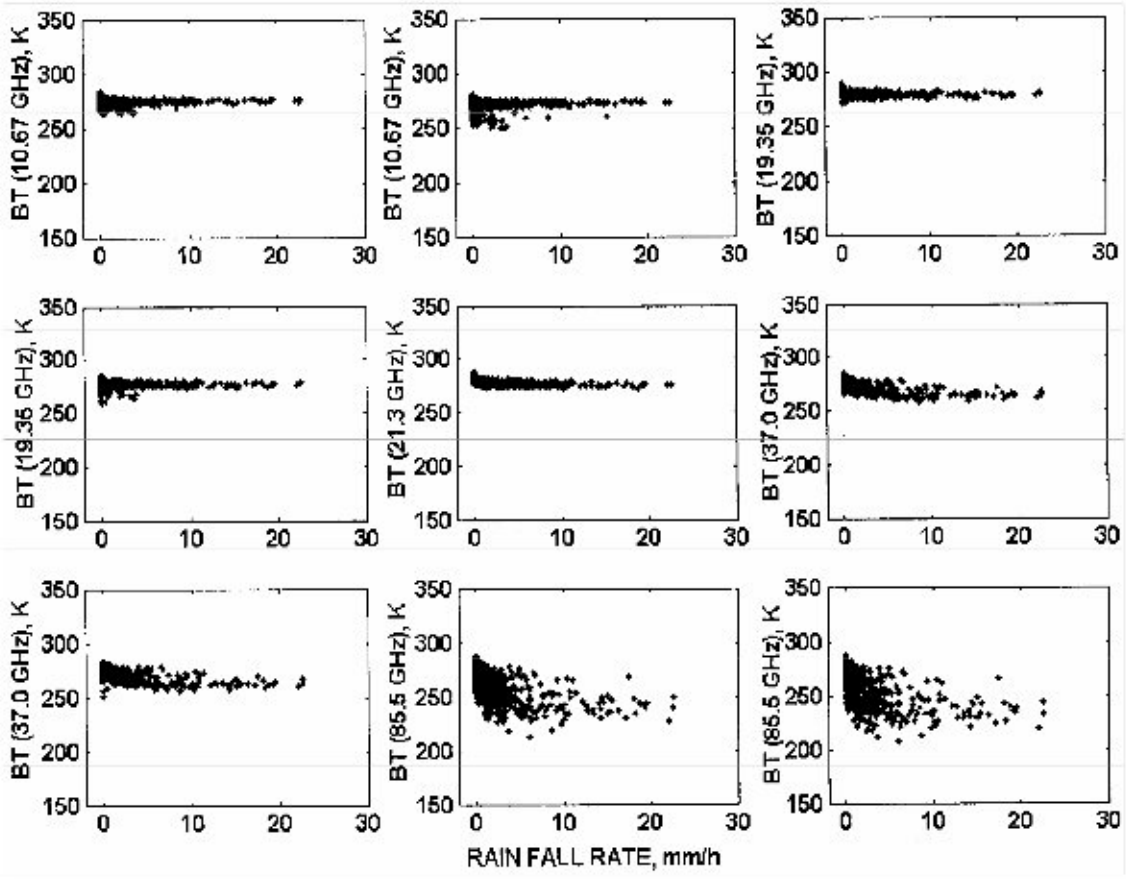

Fig. 2—Variations of BTs of nine channels with PR near-surface rain rate over land

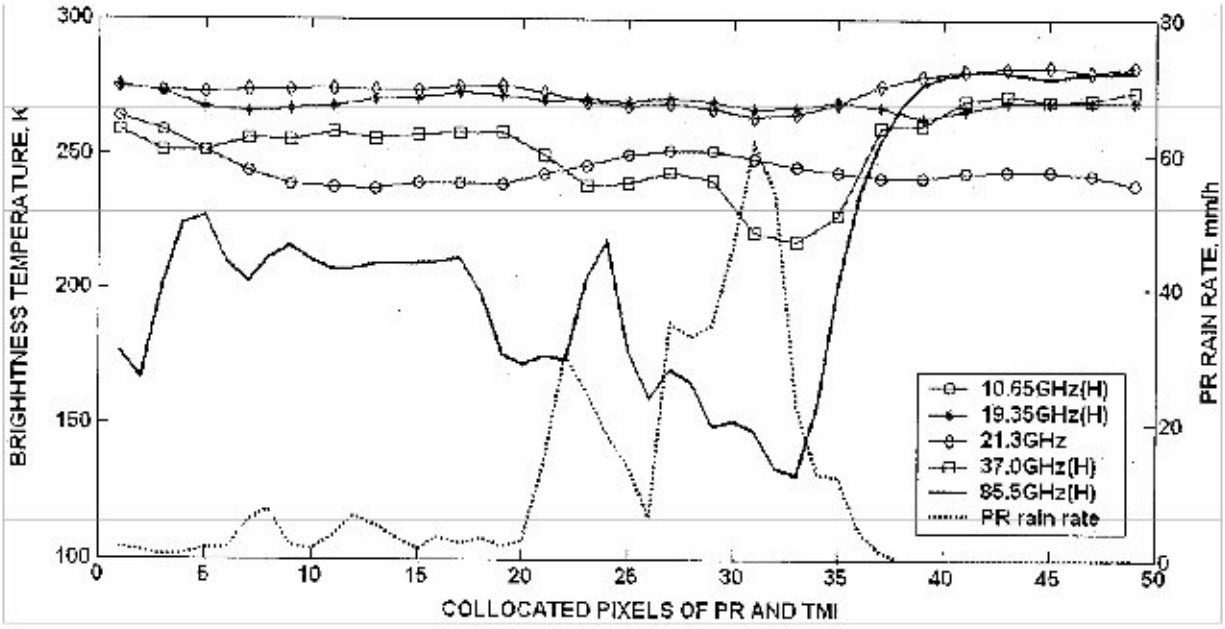

Fig. 3—Spatial variation of BTs for all frequencies with PR near-surface rain rate

channels over ocean [Fig. 4 {(a)–(d)}] and over land [Fig. 4{(e)-(h)}], respectively. Polarization difference of vertical and horizontal channels can also be noticed clearly. Figure 4 [(a) and (b)] shows polarization difference of ~70 K between the two 10.67 GHz channels over ocean. Over land, the nearly zero slope is observed for the 10.67 GHz channels [Fig. 4 (e) and 4 (f)]. For 85.5 GHz channels, polarization difference is high over ocean compared to that over land. Linear fitting of BT at this frequency shows a polarization difference of ~10 K and ~3 K over ocean and land, respectively {Fig. 4 [(c), (d) and (g), (h)]}. But the BT

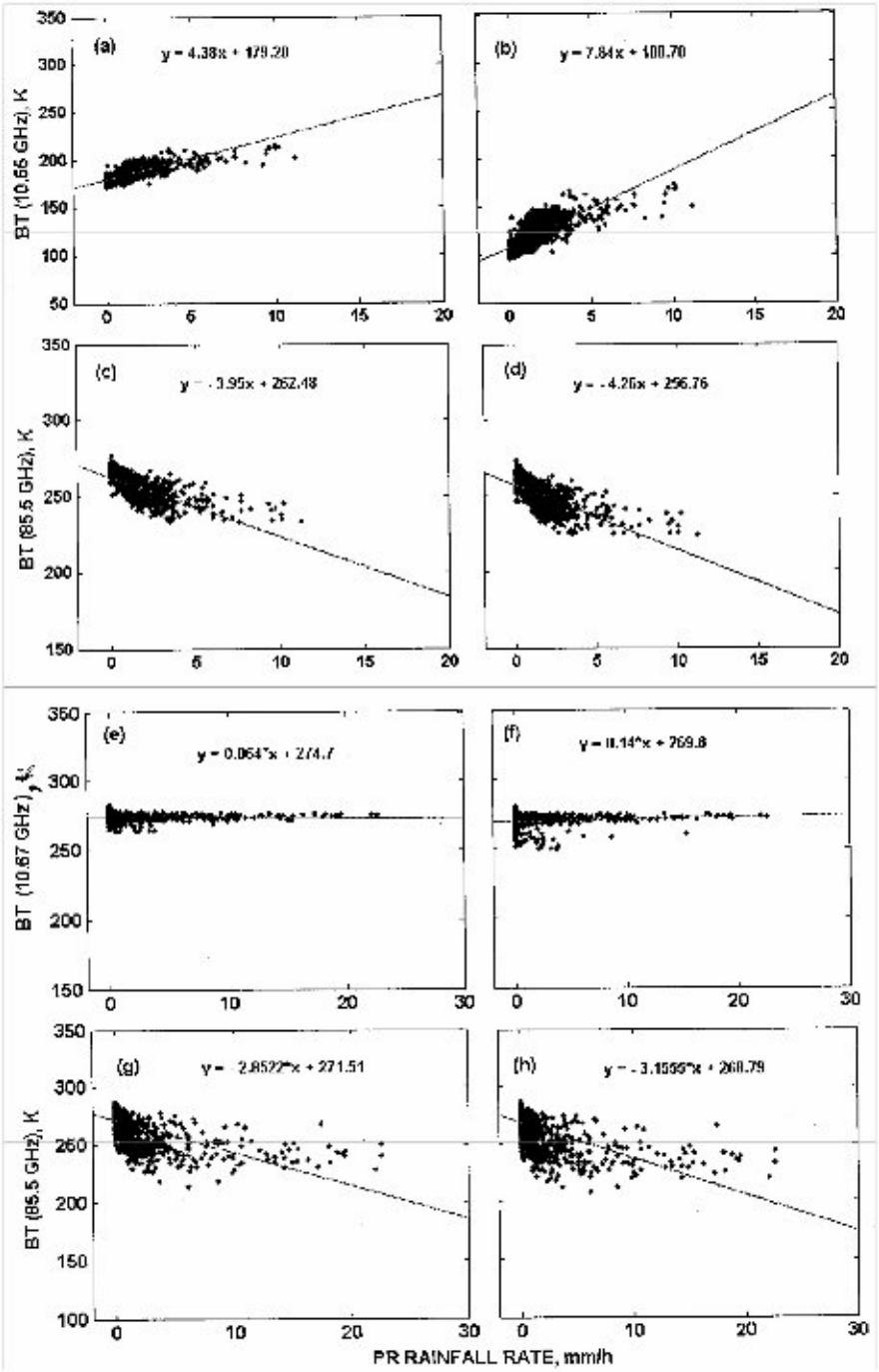

Fig. 4—Linear fitting of BT values over ocean for (a) 10.67 GHz vertical, (b) 10.67 GHz horizontal, (c) 85.5 GHz vertical, (d) 85.5 GHz horizontal and linear fitting of BT values over land, (e) 10.67 GHz vertical, (f) 10.67 GHz horizontal, (g) 85.5 GHz vertical and (h) 85.5 GHz horizontal polarization

gradient is approximately the same over ocean and land. It can also be seen that for 85.5 GHz channels BT value is less over ocean than over land by about 10 K. One point to be noted here is that, over ocean, the 10.67 GHz horizontal channel has the maximum BT gradient showing maximum dependency of this channel with rain rate [Fig. 4 (b)]. Polarization difference at a given temperature is largely a function of the visibility of polarized emission of ocean surface through and between rain clouds. Among other things, polarization information may be used to eliminate the ambiguity associated with cold BT, which may be due to either polarized emission from unobscured ocean surface or to nearly unpolarized scattering from frozen precipitation aloft[21]. The above-mentioned linear fitting shows the differences of BT values and the corresponding changes with respect to polarization over ocean and land.

4 Retrieval of rainfall rate

Retrieval of rainfall rate is affected by the spatial and temporal variations of BT values. As for example, the spatial variation is very high with resolution of about 60 km for the 10.67 GHz channel. Therefore, it is necessary to include the spatial and temporal variations of BT in the retrieval methodology. These variations of BT are incorporated in the training dataset. The BT value is measured as effective field of view (EFOV) as defined in Kummerow *et al.*[2] which has a cross-track resolution of ~ 4.6 km for the 85.5 GHz channels and 9.1 km for the other channels. Thus, PR rain rate is averaged both in cross-track and down-track directions so as to represent the appropriate value for the corresponding BT values. To incorporate the spatial and temporal variations of BT, collocated BT and PR pixels over their common swath of observations dataset are prepared from a large area of about 10000×10000 km^2 with different orbit numbers and during different time periods. Here in this study, an attempt has been made to incorporate BT values for different situations, namely convective and stratiform. Thus, the training dataset comprises all kinds of rain rate from low (0.1 mm/h) to high value (45 mm/h). As BT values tend to saturate for very high rain rate, we opted for 45mm/h as the upper limit. In the dataset, number of moderate rain rate is dominated with ~77 % data from low and moderate rain (1-15 mm/h) and ~15% data from high rain (>15 mm/h) and the remaining data are from non-raining pixels. One reason for this is that only the collocated pixels of TMI and PR have been considered and also PR pixels are averaged to match the TMI pixels.

For the present study, ANN technique is applied to retrieve instantaneous rainfall rate from TMI BT data over ocean and land. The BT data are considered as input and the collocated near-surface rain rates from PR are considered as target. The ANN has the advantage that it does not require prior knowledge of the phenomenon under study, and they almost always converge to an optimal solution. During training phase, they are capable of recognizing all the necessary relationship controlling the process and can handle massive amounts of data. For the rain rate retrieval, the multilayer perceptron (MLP) architecture is utilized. A simple MLP neural network architecture is shown in Fig. 5. It consists of one input layer, two hidden layers and one output layer. Different MLPs are trained for BTs input data over ocean as well as over land separately. Performances of the networks are validated with BT data that are not the part of the training dataset.

4.1 Artificial neural network (ANN)

The ANN is the highly interconnected, interactive data processing unit. Nodes of each layer are connected by weights, which change with the output error according to the gradient descent rule. Each of the input is multiplied by an initialized weight matrix, which gives responses at each of the hidden nodes. These responses are then multiplied by a transfer function. Transfer function utilized in the present architecture is a sigmoid function of the form:

$$F(s) = 1 / [1+\exp(-s)] \quad \ldots (1)$$

In the present case, inputs as well as the output are positive. Therefore, data are normalized so as to have values between 0 and 1. For an input variable p with maximum p_{max} and minimum p_{min} the normalized value p_n is calculated as

$$p_n = (p - p_{min})/(p_{max} - p_{min}) \quad \ldots (2)$$

The main objective for normalizing the input and output data is to ensure that the network has similar sensitivity to changes in various inputs and corresponding output of different ranges of values.

4.2 Training of the networks

For training purpose, Levenberg-Marquardt algorithm is used in this study. The main advantage of

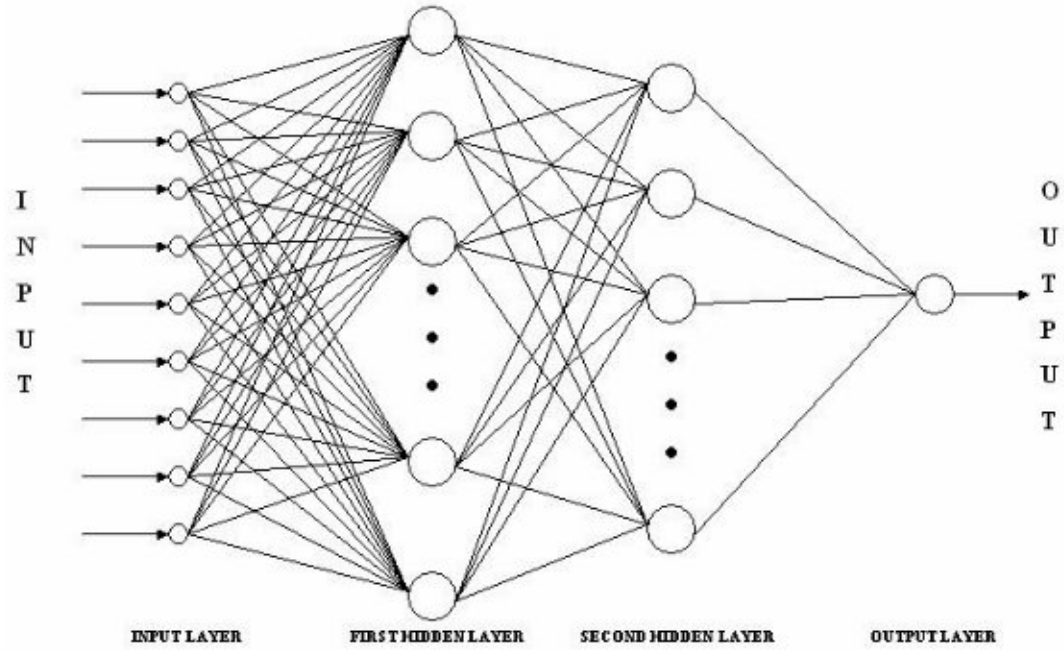

Fig. 5—An MLP architecture for rainfall retrieval

using this algorithm is that it converges quickly as compared to most of the other training algorithms[22]. It can train any network as long as its weight, net input and transfer functions have derivative functions.

There are many variations of backpropagation algorithms. The simplest implementation of backpropagation is the learning and updates of the network weights and biases in the direction in which the performance function decreases more rapidly (the negative gradient). Weight is updated as

$$w_{ik}^{t} = w_{ik}^{t-1} - \eta \frac{\partial E_k}{\partial w_{ik}} \quad \ldots (3)$$

where w_{ik}^{t} is the new updated weight at t^{th} iteration, w_{ik}^{t-1} the weight at $(t-1)^{th}$ iteration, E_k is the error at the output node *(k)* and η is the learning rate.

For Levenberg - Marquardt (LM) algorithm, the performance index to be optimized is defined as

$$F(w) = \sum_{p=1}^{p} \left[\sum_{k=1}^{k} (d_{kp} - o_{kp})^2 \right] \quad \ldots (4)$$

where $w = [\, w_1\ w_2\ \ldots\ w_N]^T$ is the weight vector consists of all weights of the network, d_{kp} and o_{kp} are the desired and output values of k^{th} output and p^{th} feature, N is the number of the weights, p the number of features and k the number of the neural network output.

The LM is designed to approach the second order training speed without computing the Hessian matrix. The LM algorithm uses the approximation to the Hessian matrix in the following Newton-like update, where the weight and biases vector **X** is updated as

$$\mathbf{X}_{t+1} = \mathbf{X}_t - [\mathbf{J}^T\mathbf{J} + \mu\mathbf{I}]^{-1}\, \mathbf{J}^T\mathbf{E}_t \quad \ldots (5)$$

where **J** is the Jacobian matrix that contains first derivatives of the network error with respect to weight and biases, **I** the identity unit matrix, **E** the error at the output and μ the learning parameter. When $\mu = 0$, it becomes the Gauss-Newton method. For very large value of μ, LM algorithm becomes the steepest gradient with a small step size. The LM algorithm requires computation of Jacobian **J** matrix at each iteration step and the inversion of $\mathbf{J}^T\mathbf{J}$ square matrix, the dimension of which is $N \times N$, where N is the number of the weights. Bias vector is a set of values added to the activation of a neuron and its dimension is same as the number of input. Backpropagation is used to calculate the Jacobian **JX** of performance with respect to the weight and bias variables **X**. Each variable is adjusted according to Levenberg-Marquardt,

$$\mathbf{JJ} = \mathbf{JX} \times \mathbf{JX} \quad \ldots (6)$$

$$\mathbf{Je} = \mathbf{JX} \times \mathbf{E} \quad \ldots (7)$$

$$\mathrm{d}\mathbf{X} = -(\mathbf{JJ} + \mu\mathbf{I}) / \mathbf{Je} \quad \ldots (8)$$

5 Rain rate retrieval results

5.1 MLP neural networks over ocean and land

Neural networks over ocean and land are trained using the nine channel BTs from TMI as input and the collocated PR near-surface rain rate as target value. Total number of data points considered over ocean and land are 4500 and 6600, respectively. Whole data set is divided into two parts and ¼th is considered for validation. Various networks are trained with different hidden nodes and hidden layers. Over ocean, ANN architecture 9-20-9-1 is found to be good enough to trace the non-linearity between BT and rain. Over land, the most suitable architecture is found out to be 9-25-10-1. The ANNs over ocean and land are named as ANN-Ocean and ANN-Land, respectively.

Table 1—Error statistics for training and validation set for neural networks over ocean and land (with all channels and with discarding lower frequency channels)

Learning	Neural Network	Correlation coefficient	Rmse mm/h	Bias mm/h
Training	ANN-Ocean	0.91	1.53	0.14
	ANN-Land	0.89	2.12	0.39
	ANN-Land-5	0.91	2.08	0.30
Validation	ANN-Ocean	0.92	2.26	0.26
	ANN-Land	0.80	3.54	1.00
	ANN-Land-5	0.83	2.98	1.00

Over ocean, with the aforementioned nine input dataset, network is trained and then validated with the validation set. Correlations of 0.91 and 0.92 are observed for the training and validation set, respectively. Detailed error statistics are given in Table 1. Figure 6 [(a)-(d)] shows the scatter and pixel-wise rain rate plot for both the training and validation sets. From Fig. 6 [(c) and (d)] it can be noticed that the ANN derived rain rate is following the PR near-surface rain rate.

Over land also the ANN is trained well, but performance is less than that over ocean. This is expected, because over land the variation of BTs with rain rate is less due to high emissivity of land as discussed in Sec.2. With ANN, viz. ANN-Land correlations of 0.89 and 0.80 are found for both training and validation set. Table 1 shows the different errors in terms of correlation coefficient, root mean square error (rmse) and bias values. It can be seen that, for ANN-Land, both rmse and bias values are more as compared to ANN-Ocean. Figure 7[(a) and (b)] shows the scatter plots between the ANN-Land retrieved rain rate and the desired rain rate from PR for training and validation, respectively. For both the training and validation sets pixel-wise variations of rain rate in case of ANN and PR are shown in Fig. 7[(c) and (d)]. It can be observed from Figs 2, 3 and 4 that the lower

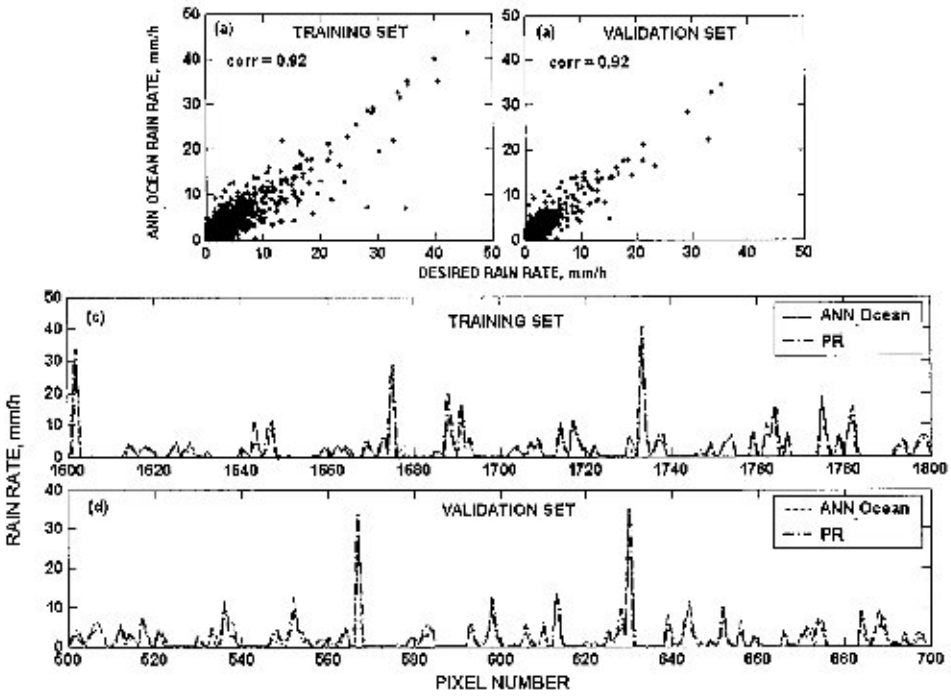

Fig. 6—Scatter plots of ANN-Ocean versus PR rain rate for (a) Training set, (b) Validation set and pixel-wise plot of rain rate, (c) Training set and (d) Validation set

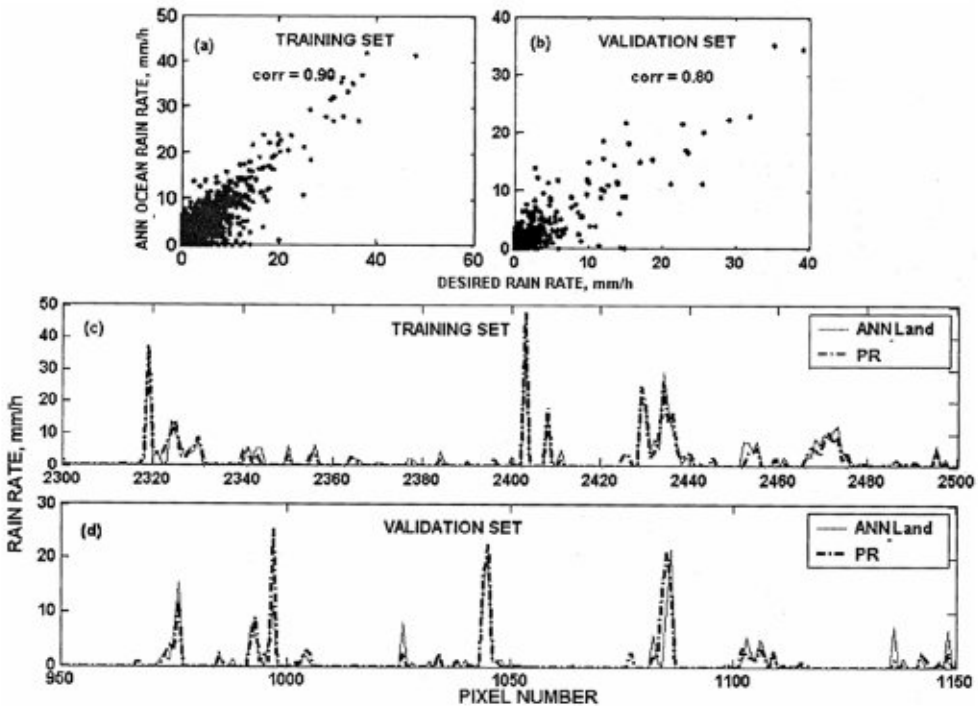

Fig. 7—Scatter plots of ANN-Land versus PR rain rate for (a) Training set, (b) Validation set and pixel-wise plot of rain rate, (c) Training set and (d) Validation set

frequency channels over land are practically not very important. It can also be noticed from Fig. 2 that the slope of the first four frequency channels over land approaches zero {Fig. 4[(e) and (f)]} as compared to other frequency channels. This shows that these lower frequency channels are nearly independent of the surface rain rate. Thus, to see the implications of the behaviour of these frequency channels over land, another MLP is trained discarding the lower frequency channels (channel Nos 1-4). It is interesting to note that this MLP performs better than the MLP with all the channels in terms of correlation coefficient and rmse. We named this MLP as ANN-Land-5. Error statistics for this MLP is given in Table 1. Scatter plots of the training and validation sets are shown in Fig. 8 [(a) and (b)]. For further testing of the developed algorithm, a comparison is made with standard 2A12 TRMM data product. Figure 9[(a) and (b)] shows the scatter plots of ANN derived rain rate and 2A12 surface rain rate over ocean and land with correlation of 0.71 and 0.57, respectively. From Fig. 9 it can be inferred that performance of ANN retrieved rainfall intensity is better over ocean than over land.

6 Summary

In this study characteristics of BTs with respect to rain rate and its implication on rainfall retrieval over ocean and land are studied. It is observed that, over ocean, the 10.67 GHz channel has the maximum dependency on surface rain rate, but over land it is least sensitive to rain rate. Over land, 85.5 GHz channel has the dependency on rain rate due to the scattering effect. Thus, these frequency channels are useful for rain retrieval over land. For 37.0 GHz channel, it is observed that over land this channel is sensitive to strong rain rate only. For low rain rate it is nearly independent. The emission effect for 37.0 GHz channel is prominent for low rain rate region over ocean, but over land it is not noticed. To see the implications of the behaviour of these channels, ANN is trained over land, discarding the channels from 1 to 4. It is observed that over land ANN performs better with five input channels as compared to the network with all the channels, in terms of both correlation coefficient and rmse. Overall, the accuracy of rain rate retrieval is more over ocean as compared to that over land. This may be due to the fact that over land, the lower frequency channels have less sensitivity towards rain rate, as land has high emissivity value.

Acknowledgements

Financial grant from the Department of Space, Govt. of India, to carry out this work [No. 10/4/362, under RESPOND Programme] is gratefully acknowl-

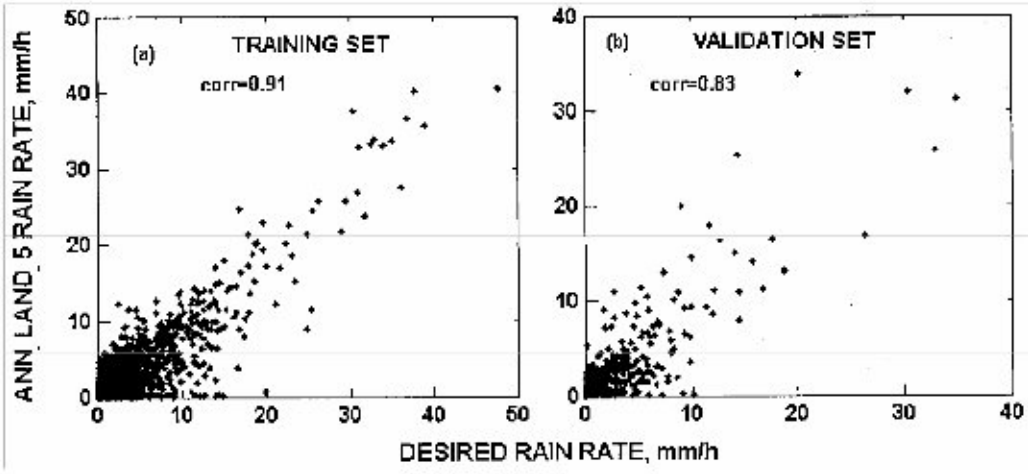

Fig. 8—Scatter plots of ANN-Land-5 versus PR rain rate for (a) Training set and (b) Validation set

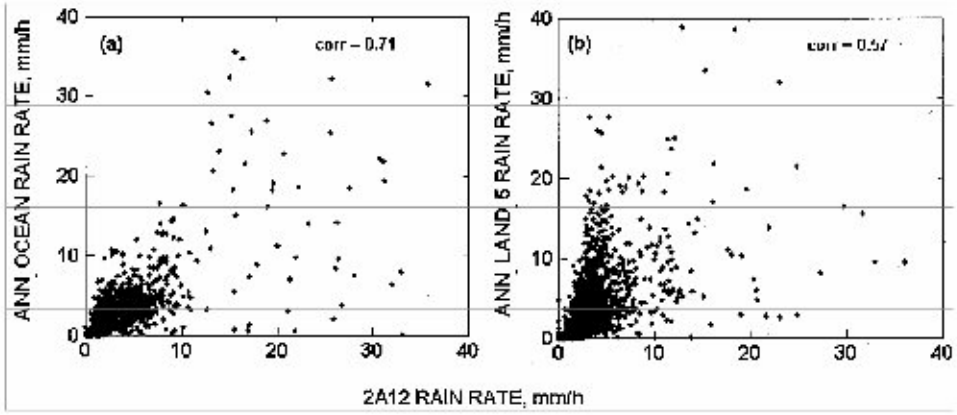

Fig. 9—Scatter plots of ANN-Land-5 derived rain rate and 2A12 surface rain rate over (a) ocean and (b) land

edged. The authors from Kohima Science College (KSC), Nagaland are grateful to the Director, Indian Statistical Institute (ISI), Kolkata, for providing the training in soft computing techniques under Electronics and Communication Sciences Unit of ISI. They are indebted to NASA-GSFC for providing the required data for the present work. Thanks are also due to the TRMM Science Data and Information System (TSDIS) help desk and Orbit Viewer team. The authors are thankful to the two anonymous reviewers for providing very constructive comments and suggestions. The authors from KSC are grateful to the authorities of Kohima Science College for providing the necessary facilities to carry out the research work. Fruitful discussion with Dr R M Gairola (Space Application Centre, Ahmedabad, India) is also gratefully acknowledged. One of the authors (DKS) would like to thank Mr Debrup Chakraborty of ISI, Kolkata and Mr Arnab Barkakati from Guwahati, Assam, for their assistance.

References

1 Ulaby F T, Moore R K & Fung A K, *Microwave Remote Sensing: Active and Passive in Microwave Remote Sensing Fundamentals and Radiometry* (Artech House, Boston, London), Vol.1, 1981, p.52.

2 Kummerow C, Barnes W, Kozu T, Shiue J & Simpson J, The tropical rainfall measuring mission (TRMM) sensor package, *J Atmos & Ocean Technol (USA)*, 15 (1998) 809.

3 Wilheit T T, Chang AT C & Chiu L S, Retrieval of monthly rainfall indices from microwave radiometric measurements using probability distribution functions, *J Atmos & Ocean Technol (USA)*, 8 (1991) 118.

4 Viltard N, Kummerow C, Olson W S & Hong Y, Combined use of the radar and radiometer of TRMM to estimate the influence of drop size distribution on rain retrieval, *J Appl Meteorol (USA)*, 39 (2000) 2103.

5 Petty G M, The status of satellite based rainfall estimation over land, *Remote Sens Environ (USA)*, 51 (1995) 125.

6 Grody N C, Classification of snow cover and precipitation using the Special Sensor Microwave/Imager (SSM/I), *J Geophys Res (USA)*, 96 (1991) 7423.

7 Petty G M, Physical retrievals of over-ocean rain rate from multi-channel microwave imaging. Part I: Theoretical characteristics of normalized polarization and scattering indices, *Meteorol Atmos Phys (Austria)*, 54 (1994) 79.

8 Kummerow C & Giglio L, A method for combining passive microwave and infrared rainfall observations, *J Atmos & Ocean Technol (USA)*, 12 (1995) 33.

9 Miller S M, Arkin P A & Joyce R J, A combined microwave/infrared rain rate algorithm, *Int J Remote Sens (UK)*, 22 (2000) 3285.

10 Gairola R M, Varma A K, Pokhrel S & Agarwal S K, Integrated satellite microwave and infrared measurements of precipitation during a Bay of Bengal cyclone, *Indian J Radio & Space Phys*, 33 (2004) 115.

11 Todd M C, Kidd C, Kniveton D & Bellerby T J, A combined satellite infrared and passive microwave technique for estimation of small-scale rainfall, *J Atmos & Ocean Technol (USA)*, 18 (2001) 742.

12 Kidd C, Result of an infrared/passive microwave rainfall estimation technique, *Proceedings of Remote Sensing Society*, USA, 1999, pp 685-689.

13 Kidd C, Kniveton D R, Todd M C & Bellerby T J, Satellite rainfall estimation using combined passive microwave and infrared algorithms, *J Hydrometeor (USA)*, 4 (2003) 1088.

14 Adler R F & Negri A J, A satellite infrared technique to estimate tropical convective and stratiform rainfall, *J Appl Meteorol (USA)*, 27 (1988) 30.

15 Bellerby T J, Todd M, Kniveton D & Kidd C, Rainfall estimation from a combination of TRMM precipitation radar and GOES multispectral satellite imagery through the use of an artificial neural network, *J Appl Meteorol (USA)*, 39 (2000) 2115.

16 Sorooshian S K, Hsu L, Gao X, Gupta H V, Imam B & Braithwaite D, Evaluation of PERSIANN system satellite-based estimates of tropical rainfall, *Bull Am Meteorol Soc (USA)*, 81 (2000) 2035.

17 Grimes D I, Coppola F E, Verdecchia M & Visconti G, A neural network approach to real-time rainfall estimation for Africa using satellite data, *J Hydrometeor (USA)*, 4 (2003) 1119.

18 Tsintikidis D, Haferman J L, Anagnostou E N, Krajewski W F & Smith T F, A neural network approach to estimating rainfall from spaceborne microwave data, *IEEE Trans Geosci Remote Sens (USA)*, 35 (1997) 1079.

19 Hsu K, Gao X, Sorooshian S & Gupta H V, Precipitation estimation from remotely sensed information using artificial neural networks, *J Appl Meteorol (USA)*, 36 (1997) 1176.

20 Kidd C, On rainfall retrieval using polarization-corrected temperature, *Int J Remote Sens (UK)*, 19 (1998) 981.

21 Petty G M, Physical and microwave radiative properties of precipitating clouds. Part I: Principal component analysis of observed microwave radiances in tropical stratiform rainfall, *J Appl Meteorol (USA)*, 40 (2001) 2105.

22 Wilamowski B M, Iplikci S, Kaynak O & Efe M Ö, An algorithm for fast convergence in training neural networks, *INNS-IEEE Int Joint Conf on Neural Networks (IJCNN 2001)*, July 14-19, Washington, DC, USA, 2001, pp. 1778-1782.